

# Energy-optimal Three-dimensional Path-following Control of Autonomous Underwater Vehicles under Ocean Currents

Niankai Yang<sup>1</sup>, Chao Shen<sup>2</sup>, Matthew Johnson-Roberson<sup>3</sup>, and Jing Sun<sup>1</sup>

**Abstract**—This paper presents a three-dimensional (3D) energy-optimal path-following control design for autonomous underwater vehicles subject to ocean currents. The proposed approach has a two-stage control architecture consisting of the setpoint computation and the setpoint tracking. In the first stage, the surge velocity, heave velocity, and pitch angle setpoints are optimized by minimizing the required vehicle propulsion energy under currents, and the line-of-sight (LOS) guidance law is used to generate the yaw angle setpoint that ensures path following. In the second stage, two model predictive controllers are designed to control the vehicle motion in the horizontal and vertical planes by tracking the optimal setpoints. The proposed controller is compared with a conventional LOS-based control that maintains zero heave velocity relative to the current (i.e., relative heave velocity) and derives pitch angle setpoint using LOS guidance to reach the desired depth. Through simulations, we show that the proposed approach can achieve more than 13% energy saving on a lawnmower-type and an inspection mission under different ocean current conditions. The simulation results demonstrate that allowing motions with non-zero relative heave velocity improves energy efficiency in 3D path-following applications.

## I. INTRODUCTION

Autonomous underwater vehicles (AUV) are essential in achieving various underwater missions (e.g., seafloor mapping [1] and underwater structure inspection [2]). It has been projected that the market size of AUVs will be doubled in the next five years [3]. Particularly, demands for scientific and commercial uses of AUVs are expected to increase significantly, calling for more reliable and energy-efficient AUV platforms [4]. To enhance the reliability and the energy efficiency of an AUV, a well-designed control system is of great importance.

Given that underwater missions typically involve following piecewise linear paths to cover a designated area, studies have been devoted to designing path-following control strategies for reliable AUV operations. For example, backstepping techniques [5] and model predictive control (MPC) [6] have been applied for two-dimensional (2D) path following of AUVs. The line-of-sight (LOS) guidance widely used in aerospace and surface vessel applications was adopted in [7]

for the 2D AUV path following under ocean currents, and an extension to the 3D path following using LOS guidance was presented in [8]. Although the above approaches can complete the mission reliably, vehicle energy efficiency is not explicitly considered.

To account for energy efficiency in control designs, optimization has been incorporated to compute vehicle thrusts by minimizing a cost function, including control efforts. For instance, a weighted sum of reference-following error and control inputs was used in [9], [10] for thrust optimization, and an economic MPC (EMPC) was proposed in [11]. An energy-optimal path-following control strategy was developed in [12], which computes yaw angle with LOS guidance law for reduced path-following error and optimizes the vehicle surge speed for energy minimization. However, the aforementioned approaches only deal with 2D motion control (i.e., in the horizontal/vertical plane).

Considering the great need to perform 3D path-following maneuvers for AUVs to achieve various underwater missions (e.g., mapping and inspection), in this paper, we extend our previous work in [12] for energy-optimal 3D path-following control under ocean currents. A two-stage controller structure is utilized. In the first stage, the vehicle propulsion energy for surge, heave, and pitch controls is first estimated and then used to compute the optimal setpoints for surge velocity, heave velocity, and pitch angle. The LOS guidance law calculates the yaw angle setpoint. In the second stage, a decoupled control is adopted to track the setpoints, where two MPCs are used to achieve the control in the horizontal and vertical planes. Extensive simulations on different mission profiles and current conditions are performed to verify the proposed approach.

## II. MODEL AND PROBLEM FORMULATION

### A. Simulation Model

An earth-fixed frame  $\{e\}$  and a body-fixed frame  $\{b\}$  are used to describe the AUV motion under ocean currents. Defined in  $\{e\}$ , the positions and orientations of an AUV is denoted as  $\eta = [x, y, z, \phi, \theta, \psi]^T \in \mathbb{R}^6$ . The velocities (relative to the ground) ( $\nu = [u, v, w, p, q, r]^T \in \mathbb{R}^6$ ), and control inputs ( $\tau \in \mathbb{R}^6$ ) are represented in  $\{b\}$ .

The following assumptions are made for modeling the effect of currents on vehicle motions: i) the currents are constant and irrotational, ii) the current velocity component in the  $z$  direction is negligible, and iii) the magnitude of currents is smaller than the maximum vehicle speed (relative to water). Note that above assumptions do not hold in general but can be satisfied in a deep-sea environment [13], which is

<sup>1</sup>Niankai Yang and Jing Sun are with the Department of Naval Architecture and Marine Engineering, University of Michigan, Ann Arbor, MI 48109, USA ({ynk, jingsun}@umich.edu).

<sup>2</sup>Chao shen is with the Department of Systems and Computer Engineering, Carleton University, Ottawa, ON, Canada. (e-mail: shen-chao@sce.carleton.ca).

<sup>3</sup>Matthew Johnson-Roberson was with Department of Naval Architecture and Marine Engineering, University of Michigan, Ann Arbor, MI 48109, USA. He is now with the Robotics Institute in the School of Computer Science, Carnegie Mellon University, Pittsburgh, PA 15213, USA. (e-mail: mkj@andrew.cmu.edu).

the designated operating environment for our testbed AUV, DROP-Sphere developed for deep ocean benthic optical mapping [14]. Based on the assumptions, the current velocities in  $\{e\}$  and the current velocities in  $\{b\}$  are then given as  $\mathbf{V}_c = [V_c^x, V_c^y, 0, 0, 0, 0]^T \in \mathbb{R}^6$  and  $\boldsymbol{\nu}_c = [u_c, v_c, w_c, 0, 0, 0]^T \in \mathbb{R}^6$ , respectively.  $\mathbf{V}_c = \mathbf{J}(\boldsymbol{\eta})\boldsymbol{\nu}_c$ , where  $\mathbf{J}(\boldsymbol{\eta}) \in \mathbb{R}^{6 \times 6}$  is the coordinate transformation matrix. The vehicle velocities relative to the current (i.e., relative velocities) are defined as  $\boldsymbol{\nu}_r \triangleq \boldsymbol{\nu} - \boldsymbol{\nu}_c = [u_r, v_r, w_r, p, q, r]^T \in \mathbb{R}^6$ .

The dynamics and kinematics of AUVs in 3D environments under currents are given by [15]

$$\dot{\boldsymbol{\eta}} = \mathbf{J}(\boldsymbol{\eta})\boldsymbol{\nu}_r + \mathbf{V}_c, \quad (1a)$$

$$\mathbf{m}_t \dot{\boldsymbol{\nu}}_r + \mathbf{f}_c(\boldsymbol{\nu}_r) + \mathbf{f}_h \boldsymbol{\nu}_r + \mathbf{f}_g(\boldsymbol{\eta}) = \boldsymbol{\tau}, \quad (1b)$$

where  $\mathbf{m}_t \in \mathbb{R}^{6 \times 6}$ ,  $\mathbf{f}_c(\boldsymbol{\nu}_r) \in \mathbb{R}^6$ ,  $\mathbf{f}_h \in \mathbb{R}^{6 \times 6}$ , and  $\mathbf{f}_g(\boldsymbol{\eta}) \in \mathbb{R}^6$  represent the vehicle total mass, Coriolis and centripetal force, hydrodynamic damping force, and hydrostatic force matrices, respectively. See [16] for the detailed expressions. Only the linear and diagonal components are considered in added mass and hydrodynamic damping matrices.

Based on the thruster allocation of DROP-Sphere, the control inputs are related to the thrusts by

$$\boldsymbol{\tau} = [T^1 + T^2, 0, T^3 + T^4, 0, (T^3 - T^4)l_1, (T^1 - T^2)l_2]^T, \quad (2)$$

where  $T^1$  and  $T^2$  are the horizontal thrusters at port and starboard,  $T^3$  and  $T^4$  are the vertical thrusters at fore and aft,  $l_1$  is the distance between vertical thrusters and the midship, and  $l_2$  is the distance between horizontal thrusters and the center line. We assume that propulsion energy accounts for the most energy use during vehicle operation. The following relationship is adopted to model the power consumption [17]:

$$h_p(T^i) = \alpha(T^i)^2, \text{ for } i = 1, 2, 3, 4, \quad (3)$$

where  $\alpha$  is the power conversion ratio.

### B. Problem Formulation

Consider that an AUV is operating in a 3D obstacle-free environment subject to currents. The paths to be followed is defined by the straight-lines connecting successive waypoints in a given set of waypoints  $\mathcal{WP} \triangleq \{\mathbf{WP}_i \in \mathbb{R}^3, i = 0, \dots, N_w\}$ , where  $\mathbf{WP}_i = (\mathbf{WP}_i^x, \mathbf{WP}_i^y, \mathbf{WP}_i^z)$  contains the  $x$ ,  $y$ , and  $z$  locations of a waypoint, and  $N_w$  is the total number of waypoints.  $\mathbf{WP}_0$  corresponds to the initial vehicle location. The objective of the 3D energy-optimal path-following control of AUVs is to find the sequences of thrusts  $\{T^i\}$  that (i) ensures the path following in 3D spaces and (ii) minimize the total propulsion energy. In this study, we assume that there will be negligible error in the knowledge of vehicle states and ocean current velocities at the vehicle location, which can be achieved using advanced sensor fusion algorithms and appropriate sensors [18].

## III. 3D ENERGY-OPTIMAL PATH FOLLOWING CONTROL

### A. Controller Architecture

Following the energy-optimal path-following control proposed in [12], a two-stage controller structure shown in

Fig. 1 is adopted. In the first stage, based on the vehicle operating condition and the paths to follow, the desired setpoints are calculated to minimize the vehicle energy and reduce the path-following error. In the second stage, given the desired setpoints, MPCs compute the thruster inputs that minimize the setpoint tracking error. By separating the thrust computation into two stages, the modularized controller structure will require lower computation, making the approach real-time feasible on resource-limited AUV platforms [19]–[21]. Meanwhile, the unmodeled dynamics neglected in the modularized design may lead to a sub-optimal solution, as we analyzed in [22].

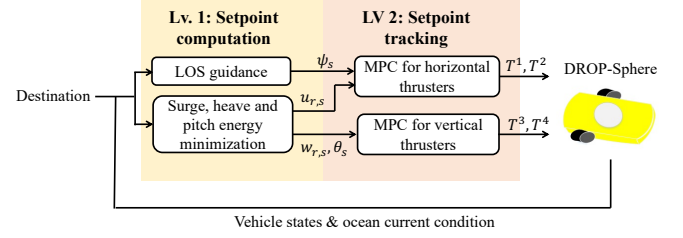


Fig. 1: Overall controller structure of the proposed energy-optimal control

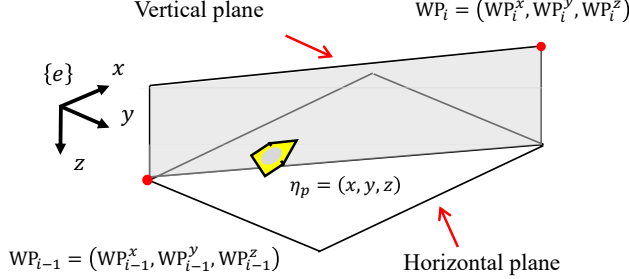
### B. Setpoint computation

For DROP-Sphere thruster allocation, four setpoints, i.e., relative surge velocity setpoint ( $u_{r,s}$ ), relative heave velocity setpoint ( $w_{r,s}$ ), pitch angle setpoint ( $\theta_s$ ), and yaw angle setpoint ( $\psi_s$ ), are required to guide the 3D motion of the vehicle. In this study, we decompose the setpoint computation into i) the yaw angle setpoint computation with LOS and ii) surge velocity, heave velocity, and pitch angle setpoint computation using optimization for the reasons as follows.

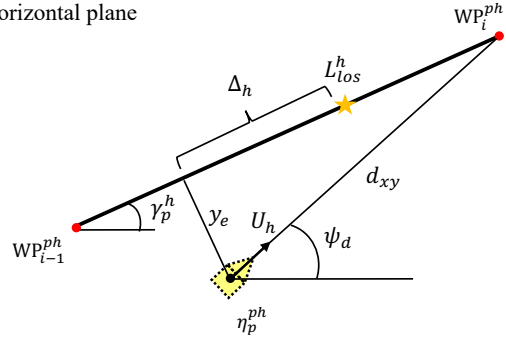
- **Natural separation of the transient and steady-state dynamics:** The energy for yaw control is spent only in transients, while the energy for surge, heave, and pitch controls is persistently consumed. Since minimal variations in the vehicle heading will be required during most mission time [15], the energy-saving potentials of optimizing the yaw motion is limited.
- **Computation load reduction:** To optimize the yaw motion, yaw dynamics must be considered, leading to increased computation and reduced real-time feasibility.
- **Handling the underactuation:** Given that the vehicle is underactuated in the horizontal plane (i.e., no control for sway motion), designing control for path following is inherently challenging. The decomposition facilitates the use of some well-established approaches, e.g., LOS guidance [8], to handle the underactuation by properly choosing the yaw angle setpoint.

1) **Yaw angle setpoint computation:** The geometry of the LOS guidance in the horizontal plane is illustrated in Fig 2(b). Mimicking the behaviors of a hemlsman, the LOS guidance drives a vessel towards an LOS position to ensure the path convergence [23]. Given a path between the waypoints to visit and the last-visited waypoint, the LOS

(a) Geometry in 3D space



(b) Horizontal plane



(c) Vertical plane

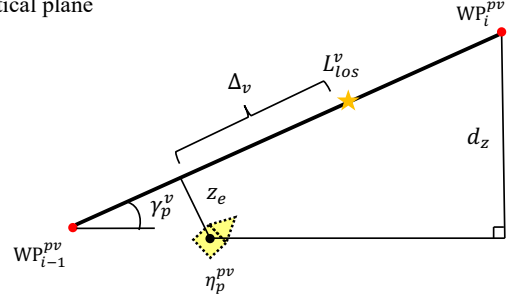


Fig. 2: Illustration of the horizontal plane, the vertical plane, and the LOS guidance.  $(\cdot)^{ph}$  and  $(\cdot)^{pv}$  denotes the projection of a (3D) point onto the horizontal and vertical plane, respectively.

position in the horizontal plane ( $L_{los}^h$ ) is defined as a point located on the path at a lookahead distance ( $\Delta_h$ ) ahead of the vehicle's projection onto the path. The LOS guidance law then computes the yaw angle setpoints under currents as follows [8].

$$\psi_s = \gamma_p^h - \tan^{-1}(y_e/\Delta_h) - \beta, \quad (4)$$

where  $\gamma_p^h = \text{atan2}(\text{WP}_i^y - \text{WP}_{i-1}^y, \text{WP}_i^x - \text{WP}_{i-1}^x)$  is the path-tangential angle in the horizontal plane, the function  $\text{atan2}$  returns an arc tangent angle from  $-\pi$  to  $\pi$ , the cross-track error  $y_e = -(x - \text{WP}_{i-1}^x) \sin \gamma_p^h + (y - \text{WP}_{i-1}^y) \cos \gamma_p^h$  is the distance from the vehicle location to the path, and  $\beta = \text{atan2}(v_r + v_c, (u_r + u_c) \cos \theta + (w_r + w_c) \sin \theta)$  is the sideslip angle under currents.

**2) Relative surge velocity, relative heave velocity, and pitch angle setpoint optimization:** To optimize the relative surge velocity, relative heave velocity, and pitch angle setpoints, a parameterization of the vehicle energy will be required. The following assumptions are made to derive a model for approximating energy consumed: 1) The roll and sway motion is negligible, i.e.,  $\dot{p} = p = \phi = \dot{v}_r = v_r = 0$ ; 2) The surge, heave, pitch, and yaw dynamics are in steady-state, i.e., constant  $u_r$ ,  $w_r$ ,  $\theta$ , and  $\psi$ . The second assumption generally does not hold for arbitrary 3D motion, but it holds approximately in deep-sea survey or mapping missions, as discussed early in Section III-B.

Based on the above assumptions, the simplified vehicle model is given as

$$T^1 + T^2 = (W - B) \sin \theta + X_u u_r, \quad (5a)$$

$$T^3 + T^4 = (W - B) \cos \theta + Z_w w_r, \quad (5b)$$

$$(T^4 - T^3)l_2 = (z_b B - z_g W) \sin \theta, \quad (5c)$$

$$\dot{z} = -\sin \theta u_r + \cos \theta w_r, \quad (5d)$$

where  $W$  is the vehicle weight, and  $B$  is the vehicle buoyancy. For DROP-Sphere,  $W < B$ , i.e., the vehicle is positive buoyant.  $X_u$  and  $Z_w$  are the surge and heave drag coefficients, respectively.  $z_b$  and  $z_g$  are the  $z$  locations of the buoyancy center and gravity center, respectively. Since the yaw motion is in steady-state, i.e.,  $T^1 = T^2$ , the thruster inputs can be approximated by solving (5) as

$$T_a^1 = T_a^2 = \frac{1}{2}((W - B) \sin \theta + X_u u_r), \quad (6a)$$

$$T_a^{3,4} = \frac{1}{2}((W - B) \cos \theta + Z_w w_r) \mp \frac{1}{2l_2}((z_b B - z_g W) \sin \theta). \quad (6b)$$

Using (3) and (6), the power consumption of all thrusters is then computed as

$$P^t = \sum_{i=1}^4 h_p(T_a^i). \quad (7)$$

For energy consumption computation, the travel time is also required, which can be approximated using the vehicle speed towards the desired waypoint [12]. Denote  $U_c$  and  $\psi_c$  as the magnitude and direction of the ocean current in the horizontal plane.  $\psi_d$  is the direction of the line between the vehicle current location and the desired waypoint (see Fig. 2(b)). The velocity component of ocean currents along and perpendicular to the line between the vehicle location and the desired waypoint are  $V_c^a = U_c \cos \psi_{cd}$  and  $V_c^p =$

$U_c \sin \psi_{cd}$ , respectively, where  $\psi_{cd} = \psi_c - \psi_d$ . The vehicle speed towards the LOS position under current then is derived as

$$U_h = \sqrt{V_{uw}^2 - (V_c^p)^2} + V_c^a, \quad (8)$$

where  $V_{uw} = \cos \theta u_r + \sin \theta w_r$  is the vehicle relative velocity along its heading in the horizontal plane. Combining (7) and (8), the vehicle energy use is approximated by

$$E(u_r, w_r, \theta, U_c, \psi_{cd}) = \frac{P^t \cdot d_{xy}}{U_h}, \quad (9)$$

where  $d_{xy} = \sqrt{(\text{WP}^y - y)^2 + (\text{WP}^x - x)^2}$  is the distance to the desired waypoint in the horizontal plane. Since the approximation in (9) considers only the energy in the steady state, the yaw control energy is not captured in (9).

The optimal relative surge velocity, relative heave velocity, and pitch angle setpoints is then computed as follows:

$$u_{r,s}, w_{r,s}, \theta_s = \arg \min_{u_r, w_r, \theta} E(u_r, w_r, \theta, U_c, \psi_{cd}), \quad (10a)$$

subject to

$$\frac{d_{xy}}{U_h} = \frac{d_z}{\dot{z}}, \quad (10b)$$

$$U_h > 0, \quad (10c)$$

where  $d_z = \text{WP}^z - z$ . The inequality constraint (10c) prevents the vehicle relative velocity along its heading from being too small so that the vehicle travel speed will always be well-defined and positive under currents. The equality constraint (10b) is meant to ensure path following. Given that constraints can not be directly imposed on the vehicle's future positions in the above optimization, we request the vehicle to take the same time to reach the desired waypoint in the horizontal and the vertical plane. Note that we allow a large path following error in (10) when the vehicle is far from the desired waypoint in the horizontal plane as avoiding drastic maneuvers after a course transition can save energy.

### C. MPC for setpoint tracking

Considering that the coupling between the vehicle dynamics in the horizontal and vertical planes can be weak [24], a decoupled control scheme is employed for the setpoint tracking to reduce the computation. The MPC for horizontal thrusters computes the left and right thrusts based on the yaw angle and relative surge velocity setpoints. The MPC for vertical thrusters takes in the pitch angle and relative heave velocity setpoints to compute the fore and aft thrusts. The MPC is chosen for two reasons. First, it can incorporate input constraints when computing the thrusts. Moreover, for DROP-Sphere, multiple thrusters are involved in 3D maneuvering. MPC has the flexibility to systematically address the multivariate optimization by formulating a proper cost.

In particular, the horizontal motion MPC is formulated as

$$\min_{\{T^1\}, \{T^2\}} \sum_{k=1}^N (\lambda_h (u_{r,k|t} - u_{r,s})^2 + (\psi_{k|t} - \psi_s)^2), \quad (11)$$

where  $(\cdot)_{k|t}$  is the  $k$ -step ahead prediction made at time

instant  $t$ ,  $N$  is the length of the prediction horizon, and  $\lambda_h$  is a constant factor penalizing the tracking error in the relative surge velocity. Note that since the yaw angle setpoint depends on the surge velocity,  $\lambda_h$  is required to be larger than 1 so that the surge motion will be stabilized first, facilitating a faster convergence to the desired waypoint in the horizontal plane. The above optimization is subject to i) thruster limits and ii) the discrete AUV dynamics in the horizontal plane assuming zero heave, roll, and pitch motion.

For the vertical motion MPC, it is formulated as

$$\min_{\{T^3\}, \{T^4\}} \sum_{k=1}^N (\lambda_v (w_{r,k|t} - w_{r,s})^2 + (\theta_{k|t} - \theta_s)^2), \quad (12)$$

where  $\lambda_v$  is a constant factor penalizing the tracking error in the relative heave velocity. The constraints for the vertical motion MPC are i) thruster limits and ii) the discrete AUV dynamics in the vertical plane assuming constant surge velocity and zero sway and roll motion.

## IV. PERFORMANCE EVALUATION

### A. Benchmark algorithm: 3D LOS-based control

The 3D LOS-based control uses the two-stage controller structure in Fig. 1. The yaw angle setpoint is determined using the LOS guidance law presented in (4), and the relative heave velocity setpoint is set to zero. The following LOS guidance law in the vertical plane is used to compute the pitch angle setpoint [8] (see Fig. 2(c) for an illustration):

$$\theta_s = \gamma_p^v + \tan^{-1}(z_e / \Delta_v) + \alpha, \quad (13)$$

where  $\gamma_p^v = \text{atan2}(\text{WP}_{i-1}^z - \text{WP}_i^z, ((\text{WP}_i^x - \text{WP}_{i-1}^x)^2 + (\text{WP}_i^y - \text{WP}_{i-1}^y)^2)^{1/2})$  is the path tangential angle in the vertical plane,  $z_e = ((x - \text{WP}_{i-1}^x)^2 + (y - \text{WP}_{i-1}^y)^2)^{1/2} \sin \gamma_p^v + (z - \text{WP}_{i-1}^z) \cos \gamma_p^v$  is the cross-track error in the vertical plane,  $\Delta_v$  is the look-ahead distance in the vertical plane, and  $\alpha = \text{atan2}(w_r + w_c, u_r + u_c)$  is the attack angle under currents. Based on the relative heave velocity setpoint (i.e., zero) and pitch angle setpoint in (13), the relative surge velocity setpoint is optimized by

$$u_{r,s} = \arg \min_{u_r} E(u_r, w_{r,s}, \theta_s, U_c, \psi_{cd}), \quad (14)$$

subject to  $U_h > 0$ . The 3D LOS-based control represents a conventional approach achieving 3D motion control, and only the surge velocity is optimized to reduce the vehicle energy consumption. The setpoint tracking of the 3D LOS-based control is the same as that proposed in Section III-C.

### B. Performance comparison

Two mission profiles are considered to compare the control approaches:

- 1) **Lawnmower-type mission:** The  $x$ ,  $y$ , and  $z$  locations of the waypoints are  $\text{WP}_i \in \{(0, 0, 0), (30, 0, 10), (30, 10, 7), (0, 10, 1), (0, 20, 2), (30, 20, 6), (30, 30, 5), (0, 30, 3)\}$   $m$  to represent a mapping mission near the sea bottom.

2) **Inspection mission:** The  $x$ ,  $y$ , and  $z$  locations of the waypoints  $WP_i, i = 0, \dots, 12$  in the inspection mission are

$$\begin{cases} WP_i^x = (7 \cos \frac{\pi(2i+9)}{6} + 7) m, \\ WP_i^y = (7 \sin \frac{\pi(2i+9)}{6} + 7) m, \\ WP_i^z = (2i) m. \end{cases} \quad (15)$$

This setup represents an inspection mission around an oil platform, e.g., spar platforms.

The vehicle is initialized with zero velocities and heading towards  $WP_1$ . The simulation is conducted in MATLAB/Simulink. A course transition will be performed once the distance between the vehicle and the target waypoint is less than 2 m. The prediction horizon  $N = 10$  steps, and the time step size  $\Delta t = 0.1$  s.  $\lambda_h$  and  $\lambda_v$  are both chosen as 50. The lookahead distance  $\Delta_h = \Delta_v = 2$  m.

The performance of two control strategies under five different flow conditions is summarized in Table I. Note that since the scale of both missions is small, the current velocities are set as constant in all simulations. The vehicle trajectories in the lawnmower-type and inspection mission for the case where  $[V_c^x, V_c^y] = [0.0417, 0.0963]$  m/s are given in Fig. 3 and Fig. 4, respectively. It can be seen that both approaches can sequentially visit all the waypoints and follow the desired paths. The proposed approach reduces vehicle propulsion energy compared to the LOS-based approach on both mission profiles under all current conditions. An average of 13.81% reduction in energy consumption is achieved. On the downside, the travel time of the proposed approach can be higher as the proposed approach only aims at minimizing energy consumption. In addition, since the proposed approach does not enforce a small depth tracking error until it is close to the desired waypoint in the horizontal plane, the depth tracking error can be large when the vehicle is far from the desired waypoint (see Fig. 3 and Fig. 4), leading to a larger 3D cross-track error.

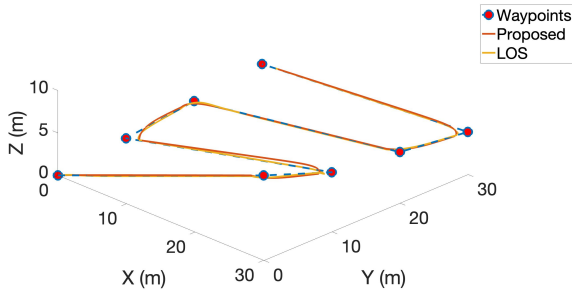


Fig. 3: Vehicle trajectory (lawnmower-type mission  $[V_c^x, V_c^y] = [0.0417, 0.0963]$  m/s)

To better understand the characteristics of an energy-efficient maneuver, the energy used to control the motion in different DOFs for the solutions in Fig. 3 is also provided in Fig. 5, which leads to the following observations:

- The proposed energy approximation can capture the major trade-off in propulsion energy during a path

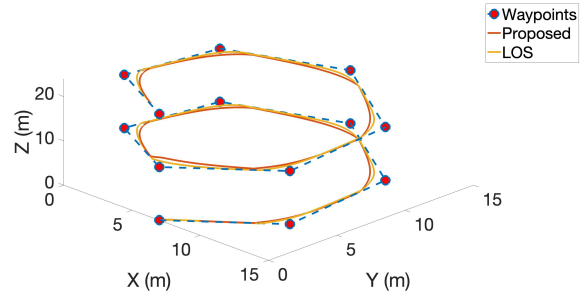


Fig. 4: Vehicle trajectory (inspection mission  $[V_c^x, V_c^y] = [0.0417, 0.0963]$  m/s)

following mission, leading to reduced energy use for surge, heave, and pitch controls.

- The proposed approach can not ensure energy reduction for yaw control as the energy approximation in (9) does not consider the yaw energy consumption.
- Employing non-zero relative heave velocities results in more energy-efficient maneuvers. Compared to the 3D LOS-based control, the proposed approach reduces energy by consuming more heave energy and less surge and pitch energy, which implies a larger heave speed, a lower surge speed, and a smaller pitch angle.

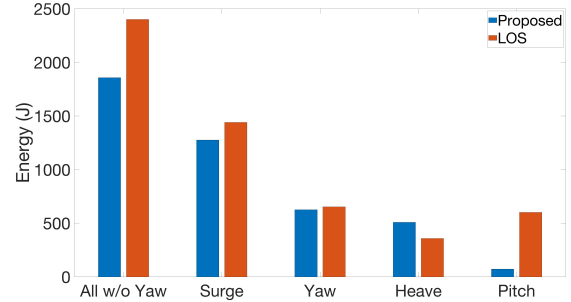


Fig. 5: Energy analysis (lawnmower-type mission  $[V_c^x, V_c^y] = [0.0417, 0.0963]$  m/s)

## V. CONCLUSIONS AND FUTURE WORK

In this paper, an energy-optimal path-following approach is proposed to control the motion of autonomous underwater vehicles in 3D spaces with ocean currents. The proposed approach computes the optimal thrusts in two stages. In the first stage, the relative surge velocity, relative heave velocity, and pitch angle setpoints are optimized by minimizing the approximated energy required to follow the path till the next course transition under ocean currents. Assuming the vehicle dynamics are negligible, the energy approximation is achieved by characterizing the vehicle thrusts and parameterizing the vehicle travel speed. The yaw angle setpoint is computed with the line-of-sight guidance law to ensure a robust path following performance under currents. Given the optimized setpoints, model predictive control (MPC) is adopted in the second stage to track the setpoints. Extensive performance evaluations are conducted on a lawnmower-type mission and a spar inspection mission under different current conditions. It is shown that the proposed approach

TABLE I: Performance comparison with the 3D LOS-based approach (the 3D cross-track error is computed by averaging the cross-track error in 3D spaces when the vehicle is away from the waypoint by 2 m)

Current condition [ $V_c^x, V_c^y$ ] (m/s)	Method	Lawnmower-type mission			Inspection mission		
		Energy	Travel time	3D Cross-track error	Energy	Travel time	3D Cross-track error
[0.0417, 0.0963]	Proposed LOS	2483.1 J	1029.5 s	0.1468 m	2093.8 J	575.3 s	0.2008 m
		3053.7 J	839.9 s	0.0782 m	2811.4 J	383.1 s	0.1250 m
[0.0841, -0.1718]	Proposed LOS	3946.7 J	704.9 s	0.1438 m	2886.8 J	391.4 s	0.2341 m
		4313.4 J	619.8 s	0.1038 m	3444.8 J	294.1 s	0.1601 m
[-0.0342, -0.0678]	Proposed LOS	2437.6 J	1209.8 s	0.0978 m	1976.9 J	673.0 s	0.1817 m
		3041.6 J	963.0 s	0.0650 m	2722.5 J	417.1 s	0.1279 m
[-0.0541, 0.1382]	Proposed LOS	3119.3 J	848.2 s	0.1534 m	2532.6 J	462.9 s	0.2323 m
		3500.1 J	704.5 s	0.1193 m	3053.8 J	332.8 s	0.1383 m
[0, 0]	Proposed LOS	1982.1 J	1490.8 s	0.1112 m	1798.2 J	834.3 s	0.1600 m
		2634.4 J	1108.9 s	0.0430 m	2488.8 J	461.5 s	0.1343 m

can achieve substantial energy efficiency improvements, an average 13% saving for the conditions considered.

In this work, only simulations are performed to verify the proposed approach. Experimental validations will be conducted in the future to further demonstrate the effectiveness of the proposed approach. In addition, the ocean currents and vehicle location are known perfectly in this study, which can be hard to achieve for some low-cost AUV platforms (e.g., DROP-Sphere). Future studies about the effects of uncertainties in the ocean currents and vehicle location on the control performance are also of great interest.

## REFERENCES

- [1] H. Zhang, L. Hao, Y. Wang, Y. Liu, Z. Wu, S. Wang, S. Shao, D. Wei, and W. Hou, "The general design of a seafloor surveying AUV system," in *OCEANS*. IEEE, 2013, pp. 1–5.
- [2] H. Kondo and T. Ura, "Navigation of an AUV for investigation of underwater structures," *Control Engineering Practice*, vol. 12, no. 12, pp. 1551–1559, 2004.
- [3] "Global autonomous underwater vehicle market research report 2020," <https://reports.valuates.com/market-reports/QYRE-Auto-38Q1152/global-autonomous-underwater-vehicle>, September 2021.
- [4] A. Palomer, P. Ridao, and D. Ribas, "Inspection of an underwater structure using point-cloud SLAM with an AUV and a laser scanner," *Journal of Field Robotics*, vol. 36, no. 8, pp. 1333–1344, 2019.
- [5] L. Lapiere and D. Soetanto, "Nonlinear path-following control of an AUV," *Ocean Engineering*, vol. 34, no. 11-12, pp. 1734–1744, 2007.
- [6] C. Shen, Y. Shi, and B. Buckham, "Path-following control of an AUV: A multiobjective model predictive control approach," *IEEE Transactions on Control Systems Technology*, vol. 27, no. 3, pp. 1334–1342, 2018.
- [7] W. Caharija, M. Candeloro, K. Y. Pettersen, and A. J. Sørensen, "Relative velocity control and integral LOS for path following of underactuated surface vessels," *IFAC Proceedings Volumes*, vol. 45, no. 27, pp. 380–385, 2012.
- [8] A. M. Lekkas and T. I. Fossen, "Line-of-sight guidance for path following of marine vehicles," *Advanced in Marine Robotics*, pp. 63–92, 2013.
- [9] C. Shen, Y. Shi, and B. Buckham, "Integrated path planning and tracking control of an AUV: A unified receding horizon optimization approach," *ASME/IEEE Transactions on Mechatronics*, vol. 22, no. 3, pp. 1163–1173, 2016.
- [10] F. Yao, C. Yang, M. Zhang, and Y. Wang, "Optimization of the energy consumption of depth tracking control based on model predictive control for autonomous underwater vehicles," *Sensors*, vol. 19, no. 1, p. 162, 2019.
- [11] N. Yang, D. Chang, M. R. Amini, M. Johnson-Roberson, and J. Sun, "Energy management for autonomous underwater vehicles using economic model predictive control," in *American Control Conference*. IEEE, 2019, pp. 2639–2644.
- [12] N. Yang, D. Chang, M. Johnson-Roberson, and J. Sun, "Robust energy-optimal path following control for autonomous underwater vehicles in ocean currents," in *American Control Conference*. IEEE, 2020, pp. 5119–5124.
- [13] Y. Liu and R. H. Weisberg, "Patterns of ocean current variability on the West Florida Shelf using the self-organizing map," *Journal of Geophysical Research: Oceans*, vol. 110, no. C6, 2005.
- [14] E. Iscar, C. Barbalata, N. Goumas, and M. Johnson-Roberson, "Towards low cost, deep water AUV optical mapping," in *OCEANS*. IEEE, 2018, pp. 1–6.
- [15] W. Caharija, K. Y. Pettersen, M. Bibuli, P. Calado, E. Zereik, J. Braga, J. T. Gravdahl, A. J. Sørensen, M. Milovanović, and G. Bruzzone, "Integral line-of-sight guidance and control of underactuated marine vehicles: Theory, simulations, and experiments," *IEEE Transactions on Control Systems Technology*, vol. 24, no. 5, pp. 1623–1642, 2016.
- [16] T. T. J. Presterro, "Verification of a six-degree of freedom simulation model for the remus autonomous underwater vehicle," Ph.D. dissertation, Massachusetts institute of technology, 2001.
- [17] N. Yang, D. Chang, M. Johnson-Roberson, and J. Sun, "Energy-optimal path planning with active flow perception for autonomous underwater vehicles," in *International Conference on Robotics and Automation*. IEEE, 2021.
- [18] Ø. Hegrenæs and O. Hallingstad, "Model-aided INS with sea current estimation for robust underwater navigation," *IEEE Journal of Oceanic Engineering*, vol. 36, no. 2, pp. 316–337, 2011.
- [19] J. Gao, A. A. Proctor, Y. Shi, and C. Bradley, "Hierarchical model predictive image-based visual servoing of underwater vehicles with adaptive neural network dynamic control," *IEEE Transactions on Cybernetics*, vol. 46, no. 10, pp. 2323–2334, 2015.
- [20] L. Guo, H. Chen, Q. Liu, and B. Gao, "A computationally efficient and hierarchical control strategy for velocity optimization of on-road vehicles," *IEEE Transactions on Systems, Man, and Cybernetics: Systems*, vol. 49, no. 1, pp. 31–41, 2018.
- [21] A. Ravi and N. S. Kaisare, "Two-layered dynamic control for simultaneous set-point tracking and improved economic performance," *Journal of Process Control*, vol. 97, pp. 17–25, 2021.
- [22] N. Yang, M. R. Amini, M. Johnson-Roberson, and J. Sun, "Real-time model predictive control for energy management in autonomous underwater vehicle," in *Conference on Decision and Control*. IEEE, 2018, pp. 4321–4326.
- [23] S.-R. Oh and J. Sun, "Path following of underactuated marine surface vessels using line-of-sight based model predictive control," *Ocean Engineering*, vol. 37, no. 2-3, pp. 289–295, 2010.
- [24] E. Y. Hong, T. K. Meng, and M. Chitre, "Online system identification of the dynamics of an autonomous underwater vehicle," in *International Underwater Technology Symposium*. IEEE, 2013, pp. 1–10.